Korean J. Chem. Eng., 38(12), 2549-2559 (2021)
DOI: 10.1007/s11814-021-0918-x

pISSN: 0256-1115
eISSN: 1975-7220

Spectroscopic, microscopic and antibacterial studies of green synthesized Ag nanoparticles at room temperature using *Psidium guajava* leaf extract

Tatan Ghosh[*,**,†], Amarnath Chattopadhyay[**], Atis Chandra Mandal[***], Subhamay Pramanik[****], Sumit Mukherjee[****], and Probodh Kumar Kuiri[****,†]**

*Department of Physics, Balarampur College, P.O.-Rangadih, Dist-Purulia 723143, West Bengal, India
**Department of Microbiology, Suri Vidyasagar College, P.O.-Suri, Dist-Birbhum 731101, West Bengal, India
***Department of Physics, The University of Burdwan, Burdwan 713104, West Bengal, India
****Department of Physics, Sidho-Kanho-Birsha University, Purulia 723104, West Bengal, India
(*Received 6 June 2021 • Revised 11 July 2021 • Accepted 3 August 2021*)

Abstract−Spectroscopic, microscopic and size dependent antibacterial efficiency of Ag nanoparticles (NPs) synthesized by green approach were studied. Five different samples of Ag NPs having average sizes in the range of ~14 to ~21 nm were synthesized using *Psidium guajava* (Guava) leaf extract (0.25 ml, 0.5 ml, 1 ml, 2 ml, 4 ml, respectively) in 50 ml aqueous $AgNO_3$ solution of molar concentration of 1 mM. The sizes of the NPs were found to increase with increase in concentration of leaf extract. Such increase in NP size is mainly due to the increase in biomolecules, in the solution, that transforms the Ag ions to Ag NPs. Spectroscopic and microscopic properties of as-synthesized Ag NPs were obtained by characterizing the prepared samples using suitable and affordable methodologies. These Ag NPs showed significant size dependent antibacterial effect. The minimum inhibitory concentration and minimum lethal concentration of the sample showing highest zone of inhibition against *Escherichia coli* (*E. coli*) was determined as 40 μg/ml and 80 μg/ml, respectively. Percentage of survivability was also measured through viable plate count. The smallest Ag NPs (average size ~14 nm) considered here produced the best antibacterial activity against the tested *E. coli* compared to Ag NPs having larger sizes at identical bacterial concentration. The enhanced antibacterial efficiency for smaller Ag NPs is mainly due to larger surface area-to-volume ratio of smaller NPs. The probable mechanism of bio-reduction of silver ions and formation of Ag NPs has also been well explained, which justifies the result obtained in this work.

Keywords: Ag Nanoparticles, *Psidium guajava* (Guava) Leaf Extract, Green Synthesis, Characterizations of Nanomaterial, Antibacterial Activity

INTRODUCTION

Metal nanoparticles (NPs) such as Pt, Pd, Au, and Ag have recently gained much attention because of their potential applications in physics, chemistry, and biology [1,2]. Among these metal NPs, Ag NPs or Ag coating system has been considered as a promising material for biomedical applications due to its cost effectiveness and high efficiency in comparison to other noble metal NPs [3,4]. Although from ancient times bulk Ag has been considered to be disinfectant agent [5], but Ag NPs have been broadly used as antimicrobial agent since 2004 [6]. It offers very high antimicrobial effects over a large range of bacteria and parasites [7]. There are numerous examples where Ag NPs were repeatedly used in different medical applications, such as imaging, hyperthermia of tumors and drug delivery [8,9]. Some recent studies also used Ag NPs as anti-cancer agent and the entire observed results show positive effects [10, 11]. The cell killing effect of Ag NPs is size and dose-dependent, as determined by the minimum inhibitory concentration (MIC) and minimum lethal concentration (MLC) against *Escherichia coli*, *Bacillus subtilis* and *Staphylococcus aureus* [12]. The antimicrobial properties of Ag NPs were found to be enhanced for smaller NPs due to large surface area to volume ratio. This is very exciting due to the upward microbial resistance to antibiotics and the development of resistant strains [13]. The fact is that smaller particles with larger surface area can actively release more Ag ions to act. Also, smaller particles have an easier route of endocytosis into cellular membranes [14]. A limited number of studies are available on NP size dependent antimicrobial efficiency of Ag NPs prepared using the green approach. Therefore, the present study of size dependent antibacterial efficiency opens a new avenue in biomedical applications of Ag NPs safely, as NPs are prepared through green synthesis approach. Ag is capable of killing both Gram positive and Gram-negative pathogens. To neutralize bacterial pathogens, coated materials that release Ag NPs were developed. Materials incorporated with Ag are categorized as releasing because of their nature of work. The released Ag ions are the actual agents which destroy microbial pathogen by a versatile mode of action, such as inhibiting DNA replication, disrupting metabolic pathways, lysis of cell membrane, and inhibiting the enzyme system [15]. Ag NPs are multi-faceted in different technologies and can be incorporated into many materials because of their functionality including antibacterial. In the field of controlled drug delivery, hydrogels can be used as a matrix for incorporating Ag NPs with useful biomedical devices for the continuous and slow release of Ag^+ [16]. Ag NPs incorporated with

†To whom correspondence should be addressed.
E-mail: tatanghosh83@gmail.com, probodh@skbu.ac.in

HPMC can also be used for the controlled release of NPs, which makes it more usable in therapeutic window. Kvitek et al. proposed a method for the preparation of such a colloidal matrix for the controlled release of Ag NPs [17]. Nanosilver coatings on fabric with multifunctional ability make it possible to create medical textile materials with multifunctional properties such as antibacterial, antimycotic, and antiseptic [18]. Surface treatment on textile material with green-synthesized Ag NPs make a product with more color fastness, UV-protection ability and antibacterial activity [19].

Many methods have been employed to produce Ag NPs, such as chemical, hydrothermal, microwave assisted method, and ion implantation [20-28]. Shahzad et al. [21,22] reported the synthesis of high and ultra-high concentrated Ag NPs with long-term stability using precursor concentration as high as 200 mM and 2,000 mM, respectively. Highly reproducible Ag nanocubes were also synthesized via chemical synthesis method [23]. Poly acrylic acid (PAA) coated Ag NPs were found to maintain their stability even after 14 months [24], whereas carboxymethylated gum kondagogu (CMGK) capped Ag NP showed huge antibacterial action with inhibition zone up to 28 mm [25]. Being a clean and having control over size and size distribution, ion implantations are also very efficient to synthesize metal, including Ag NPs embedded in different matrices with a predecided depth in the matrix [27,28]. These methods are very effective in regulating the morphology as well as the size of the NPs, but recently developed biological method for synthesizing Ag NPs using extract of different parts, such as root, leaves, and fruit of various plants and also a variety of microorganisms offer numerous benefits over the conventional methods. Use of plant extract in green synthesis is much preferable as compared to microorganisms due to its cultural hazard. Green synthesis process is economically viable, environmentally sustainable and very useful for large scale synthesis [29] without any difficulty. Moreover, this process does not demand any critical conditions, such as high energy, temperature, pressure and toxic chemicals which may have undesirable effects in medical applications. Though synthesizing sized controlled Ag NPs using leaf extract is challenging, we are reporting here five different sized Ag NPs by controlling over only the *Psidium guajava* (Guava) leaf extract on the precursor solution.

In the present study, Ag NPs were synthesized having size from ~14 nm to ~21 nm by varying the concentration of the leaf extract within precursor ($AgNO_3$) solution. The presence of different biomolecules in Guava leaf extract acts as a natural capping and reducing agent. To study the spectroscopic properties of the prepared samples, complementary techniques such as optical absorption (OA) spectroscopy, photoluminescence (PL) spectroscopy, Fourier transformed infrared (FTIR) spectroscopy, X-ray diffraction (XRD) and energy dispersive X-ray spectroscopy (EDS) were used, whereas for microscopic analysis transmission electron microscopy (TEM), electron scanning microscopy (SEM) and selected area electron diffraction (SAED) were performed. The rigorous antimicrobial efficiency of five different Ag NPs samples against *Escherichia coli* (*E. coli*) has been studied. Till now, size dependent anti-microbial effects have been poorly studied. Therefore, it is very much required to study and explore the size dependent anti-microbial effects of biogenic Ag NPs. In the present work we have systematically studied and established that smaller Ag NPs show greater antimicrobial activity than the larger NPs.

EXPERIMENTAL DETAILS

1. Synthesis of Ag NPs

Locally collected Guava leaves were washed thoroughly in running water to remove the dirt and dust on the surface of the leaves, and then cleaned in double-distilled water for several times. 5 g of washed leaves were crushed using mortar and pestle and added to 100 ml of double-distilled water before keeping it at 40^0 Celsius in a hot air oven for ~4 hours, which resulted the color of the water turning pale yellow due to the effusion of different biomolecules into the warm water from the leaf. This pale yellow leaf extract was filtered by Whatman no. 1 filter paper and stored in the refrigerator at 4^0 Celsius for experimental use as a bio-reduction of Ag ion. 250 ml of 1 mM $AgNO_3$ solution was prepared using double-distilled water. Then 0.25 ml, 0.5 ml, 1 ml, 2 ml and 4 ml of extract was added separately to 50 ml of silver nitrate solution, which were marked by S1, S2, S3, S4, and S5, respectively, and stirred by magnetic stirrer at room temperature till the color of the solution changed from transparent to pale yellow, which confirmed the formation of Ag NPs. It was also noticed that for samples having higher concentration of leaf extract, the faster is the change in color.

2. Characterizations of Ag NPs

The crystallinity of all samples was determined by XRD studies using an X-ray diffractometer (PROTO AXRD) with Cu K_α (λ= 0154.06 μm) radiation for 2θ values in the range of 30^0 to 80^0 with an interval of 0.02^0. For XRD study, films of the different samples were prepared on properly cleaned glass slides by drop casting. For this purpose, five glass slides of equal sizes (~1.5 cm×1.5 cm) were cleaned successively by soap solution, distilled water, methanol and again in distilled water followed by sonication for 15 minutes. A few drops of individual sample were put on the corresponding glass slide through a micropipette and the sample was allowed to dry at normal condition. The process of dropping and drying the sample was continued till a film of significant thickness was prepared for XRD study. The sizes of NPs in each of the samples was estimated using TEM images. The TEM studies were fulfilled using a TEM machine (JEOL, JEM 1400 plus) operating at 120 kV. The crystalline structure of the prepared sample was studied further by selected area electron diffraction (SAED) image obtained from the TEM machine. The morphology and elemental composition were determined by SEM and EDS study obtained from ZEISS, Sigma 300 system. For TEM a drop of samples was dropped through a micropipette on a copper grid coated with carbon and for SEM and EDS characterization a few drops were cast on a small aluminum plate. Optical absorption (OA) spectroscopy measurements were carried out using UV-Vis spectrophotometer (JASCO, V-630) scanned from 300 nm to 700 nm with distilled water produced by Lab Pure Series Direct Ultra TUVF-5 (Bio-Age, India) as baseline. Photoluminescence (PL) emission spectra were recorded through Cary Eclipse fluorescence spectrometer (Agilent Technologies) at an excitation wavelength of 380 nm. For FTIR spectroscopic analysis a drop of aqueous sample of Ag NPs was placed on a pellet made by KBr purchased from Sigma Aldrich Co. The FTIR data was

recorded using L1600300, Perkin Elmer, UK working between the wave number of 450 cm^{-1} and 4,000 cm^{-1} with a data interval of 1 cm^{-1}.

3. Antibacterial Studies of Ag NPs

A common assay for antimicrobial activity is the agar cup assay. An overnight grown *E. coli* culture (10^6 CFU/ml) is taken and 0.1 ml from that is spread over Mueller Hinton agar plate (Himedia lab). After the spreading is complete, the plate is allowed to dry for 5 minutes. 50 µl of different samples (S1 to S5) of Ag NPs are loaded to cups that were punched into agar plates. Plates are then incubated carefully within an incubator for 20 h at 37 °C. Ag NPs' diffusion from the cups into the surrounding agar medium makes a clear hollow zone, i.e. zone of inhibition (ZOI) due to the cessation of bacterial growth in the surrounding area of the cup. Diameter of these zones is measured in mm by a metric ruler [30]. To study how good the antibacterial agent of our sample was over chemically synthesized PVP capped sample, a comparison study was performed. For this a similar agar plate was prepared after 24 hours in which highest antibacterial effect produced Ag NPs sample, aqueous $AgNO_3$ (concentration 1 mM), Guava leaf extract, chemically synthesized PVP capped Ag NPs (having same precursor concentration) and PVP are loaded and the above mentioned process is repeated.

The minimal inhibitory concentration (MIC) along with minimum lethal concentration (MLC) was determined by a modified tube-dilution method as described by Willey et al. [31]. A series of Mueller Hinton broth tubes containing Ag NPs concentrations of 10, 20, 40, 60, 80, 100 and 120 µg/ml were inoculated with 0.1 ml of 10^6 CFU/ml culture of *E. coli*. The lowest Ag NP concentration resulting in no growth in terms of turbidity after proper incubation was the MIC. The process also included a positive control (nutrient media with culture) and a negative control (nutrient media with Ag NPs).

To find MLC, the tubes showing no growth were then cultured into fresh agar plate and incubated at 37 °C for 24 h. The lowest concentration from which the test organisms do not grow was the MLC.

For viable plate count [32], two nutrient agar plates were prepared and sterilized, then one plate with *E. coli* (test 1) and a second plate with Ag NPs treated *E. coli* (test 2) were spread on. For test 1, 0.1 ml distilled water was mixed with 0.1 ml of 10^{-4} diluted *E. coli* culture and for test 2, 0.1 ml S1 Ag NP sample was mixed with 0.1 ml of same diluted *E. coli* culture. Both test samples were kept for 10 minute at room temperature, after which spreading was done. Then both the plates were incubated overnight at 37 °C. On next day after 24 hours colony numbers were counted and the values converted into colony forming units (CFU/ml). The survival percentage of the tested bacterial cells was calculated by simply dividing the CFU/ml of treated cell by CFU/ml of untreated cell and multiplying 100. Experiments were performed in three sets.

RESULTS AND DISCUSSION

1. Structural Analysis

1-1. XRD Studies

To study the crystalline structure of the synthesized samples XRD measurements were carried out. The production of Ag NPs of all the five samples was confirmed from the XRD spectra as shown in Fig. 1(a)-(e). For the sample having leaf extract concentration of 0.25 ml, four peaks at 38.34^0, 44.51^0, 64.68^0, and 77.62^0 in 2θ value, which correspond to the characteristic face-centered-cubic (fcc) Ag crystalline planes of (111), (200), (220), and (311), respectively [33]. These planes are marked in the figure. Out of all these planes, the dominant one is (111), which indicates Ag particles grow preferably in this plane to achieve minimum surface energy. For all other samples, depending upon the leaf extract concentration, the peak positions are found to shift slightly. Apart from these characteristics peaks there are some other unmarked peaks in the XRD spectra of all the five samples. The appearance of these unmarked peaks may be due to impurities present in the sample or may be related to crystalline and amorphous organic phase of the biomolecules present in Guava leaf extract, which act as reducing and capping agents here. These observations are very close to the study of Siddhant et al. [34]. In addition to the peak shift, the full width at half maximum (FWHM) as measured from the XRD peaks decreases with increase in concentration of Guava leaf extract. This reduction of FWHM with increase in concentration of leaf extract indicates the growth of Ag NPs. The FWHM corresponding to (111) planes were found to be 0.63 0.57, 0.54, 0.49 and 0.45 degrees for S1, S2, S3, S4 and S5 samples, respectively. Using these XRD data, we could estimate the size of the Ag particles following Debye-Scherrer formula [35]:

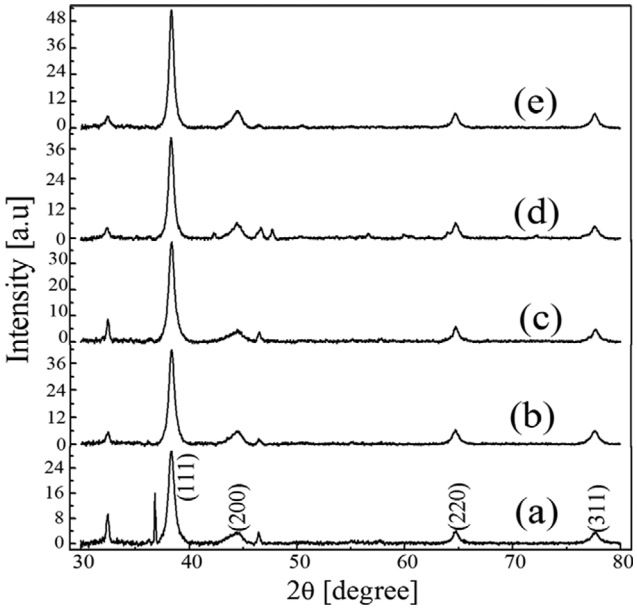

Fig. 1. XRD spectra of Ag NPs for different concentrations of Guava leaf extract. (a)-(e) are for samples S1-S5, respectively.

$$D = \frac{0.94\lambda}{\beta\cos\theta} \quad (1)$$

Here λ stands for the wavelength of x-ray used, θ is for the angle of diffraction of a characteristic XRD peak and β is for the corresponding FWHM (in radian) at θ. Using the aforesaid equation the average sizes of the Ag particles were found to be about 14 nm, 15.5 nm, 16.2 nm, 17.8 nm, and 19.5 nm corresponding to leaf extract

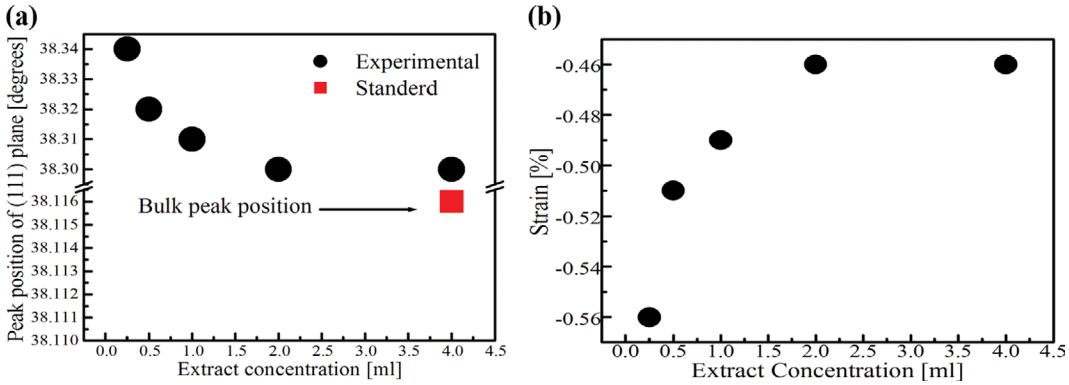

Fig. 2. Variations of (a) XRD peak position of (111) plane and (b) percentage of strain for the same plane as a function leaf extract.

concentrations of 0.25 ml, 0.5 ml, 1 ml, 2 ml, and 4 ml, respectively. Thus, it is clearly indicated that Ag NP's size increases as one increases the concentration of leaf extract. If extract concentration is increased, the number of biomolecules present in that extract also increases, which in turn affects the formation of Ag NP in a way that increases the size of Ag NP by providing too many electrons for faster nucleation and rapid reduction of Ag^+ to Ag^0.

Another important aspect of the XRD spectra is that there is peak shift corresponding to (111) plane towards the higher value of 2θ as compared to standard bulk Ag. Similarly, the crest positions of other planes of all the five samples are also shifted towards higher value of 2θ. This peak shift has an inverse relation with the particle size. The origin of this shift in the peak position in comparison to its bulk twin is because of the presence of strain, in the small particles, which developed during its formation. In Fig. 2(a) the variation of peak position of (111) plane with leaf extract concentration is plotted. Here in the same figure the crest position of (111) plane of bulk Ag is shown as filled square. As long as the concentration of leaf extract increases, the 2θ value of peak position decreases and finally approaches toward the bulk peak position. The strain is compressive or tensile if the shift in XRD peak position occurs towards higher diffraction angle or lower diffraction angle, respectively [36]. Here, for all the samples the strains are seen to be compressive as the shift in peak position is in the higher angle side. Quantitatively, percentage of strain (ε) developed in the nanocrystals is given by [37]:

$$\varepsilon = \frac{d - d_0}{d_0} \times 100\%, \quad (2)$$

where d is the separation among the sets of parallel planes of the Ag NPs and d_0 is the unstrained bulk lattice spacing. The variation of ε for characteristics plane (111) with the leaf extract concentration is depicted in Fig. 2(b). For all the five samples ε is negative, indicating that the strain is compressive. Initially, the strain decreases rapidly with the increase of leaf extract concentration and then finally attains almost saturation value. The decrease in strain is because of the growth of the particle in size [38].

1-2. TEM and SAED Studies

The TEM images of all the samples are shown in Fig. 3(a)-(e). The histograms corresponding to each of the images are given just right of it. In all the images, the Ag NPs are found to be nearly spherical. For lowest concentration of juice of Guava leaf (sample S1), the NP size ranges from 11 nm to 17 nm with an estimated average size of ~13.8 nm. For all other cases except the highest concentration of leaf extract (sample S5), the NP size ranges from ~9 nm to ~21 nm with average sizes of ~14.6 nm, ~16 nm, and ~17 nm, respectively. For highest concentration, the Ag NP size distribution is found to be a very narrow (20.1 nm to 21.5 nm) with average size of ~21 nm. Importantly, this concentration of leaf extract leads to the evolution of closely monodispersed NPs, which is very much desirable in many practical applications. In the histograms we notice also that there is a systematic shift of the average size of Ag NPs toward higher value. This result is consistent with the average size of the Ag NPs as estimated from XRD data. The average sizes of the Ag NPs as estimated from XRD and TEM studies are displayed in Table 1. Both studies show nearly equal values of average NP sizes for each concentration of leaf extract.

Table 1. Comparison of estimated average sizes of Ag NPs as obtained from TEM and XRD analysis. Standard deviations are given in parentheses next to each value

Concentration of leaf extract (ml)	Average size from XRD (nm)	Average size from TEM (nm)
0.25	14(0.9)	13.8(2)
0.50	15.5(1.1)	14.6(2)
1.00	16.2(1.2)	16(2)
2.00	17.8(1.5)	17(2)
4.00	19.5(1.7)	21(1)

Fig. 4 shows the variation of average NP size as a function of concentration of leaf extract. Here the NP sizes were considered from the TEM studies. It is observed that the average size of Ag NPs increases with increase in leaf extract concentration. Initially, the variation is fast then it varies slowly.

SAED pattern was also obtained through the TEM machine used to study further the crystalline structure of the sample. Fig. 5 shows the SAED image corresponding to the sample S1. The four diffraction rings as marked in the figure correspond to the first four diffraction planes of Ag NPs as observed in XRD spectra. The distinct diffraction rings in the SAED pattern of the sample confirm the synthesized Ag NPs are well defined and crystalline. The inverse of the radius of a particular ring in the SAED image gives the inter-

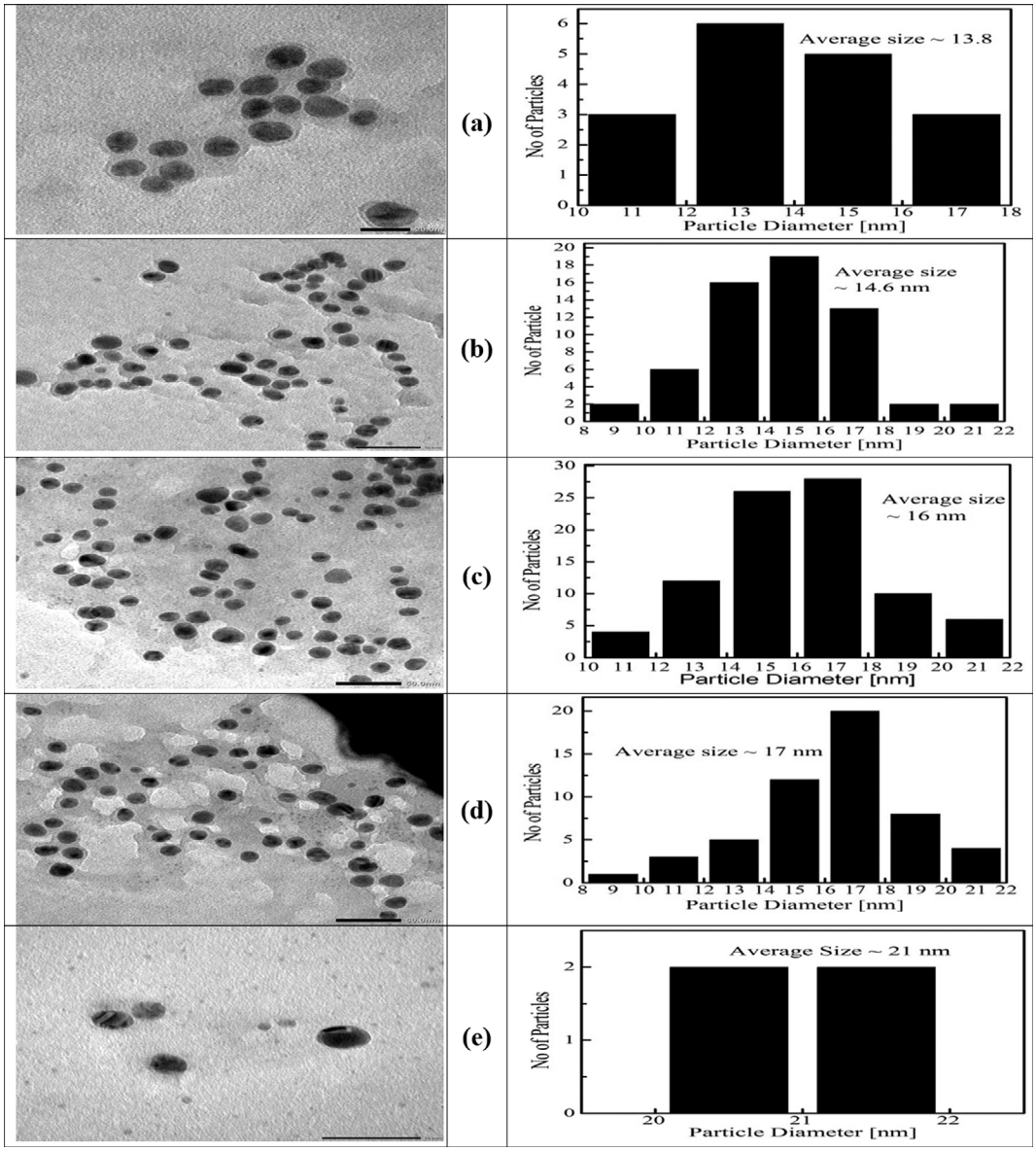

Fig. 3. TEM images of the Ag NPs for different concentrations of leaf extract. (a)-(e) correspond to the samples S1-S5, respectively. The histograms just right side of each of the TEM images show the NP size distributions. The scale bar for TEM image (a) is 20 nm and the rest are 50 nm.

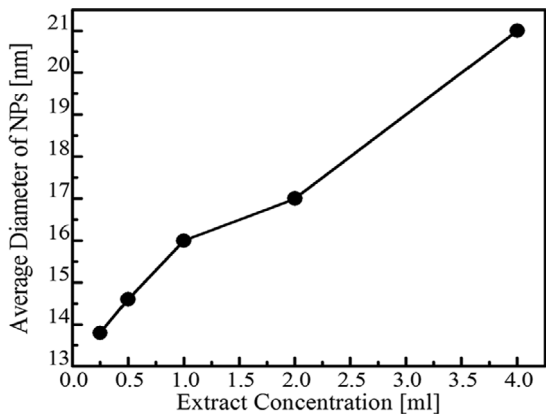

Fig. 4. Variation of average size of NPs as a function of concentration of leaf extract. Solid line is to guide the eye.

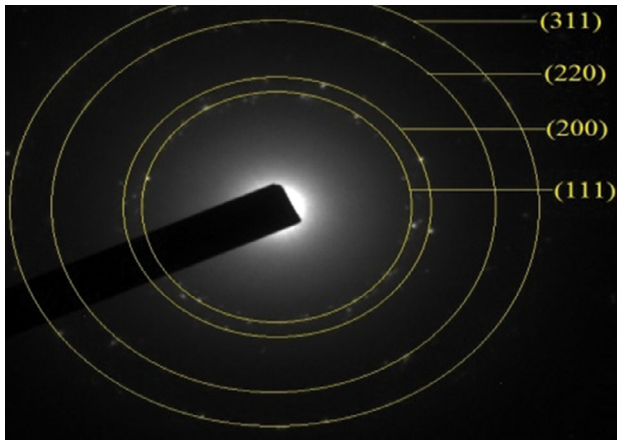

Fig. 5. SAED image of Ag NPs corresponding to the sample S1.

Table 2. Comparison of interplanar distance (d) and lattice constant (a) for the first four diffraction planes of Ag NPs measured from SAED and XRD experiments, respectively, along with standard value

Diffraction plane (hk*l*)	SAED measurement		XRD measurement		Standard value	
	d (nm) 1/radius of the ring	a (nm) using Eq. (2)	d (nm) using Eq. (3)	a (nm) using Eq. (2)	d (nm) Ref. [40]	a (nm) Ref. [39]
(111)	0.2447	0.4238	0.2345	0.4061	0.2359	
(200)	0.2151	0.4302	0.2033	0.4066	0.2044	4.085
(220)	0.1501	0.4245	0.1440	0.4072	0.1445	
(311)	0.1273	0.4222	0.1229	0.4076	0.1231	

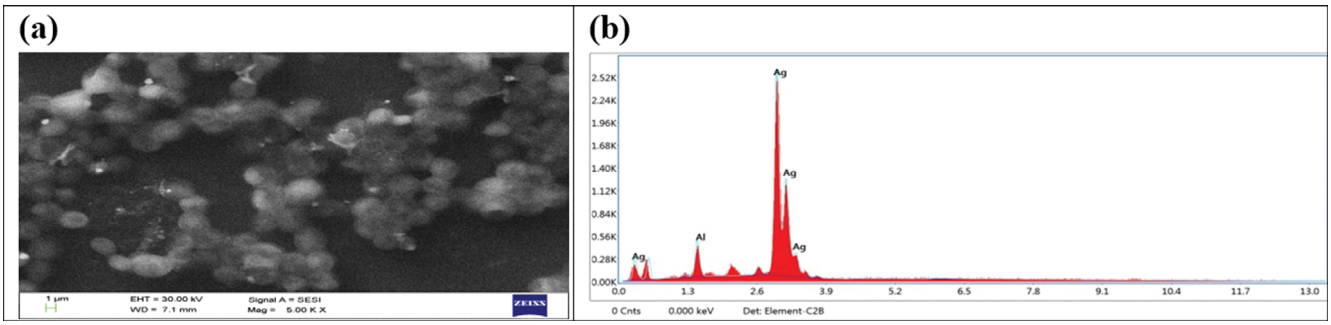

Fig. 6. (a) SEM image and (b) EDS spectrum corresponding to the sample with highest concentration of leaf extract.

planar distance (d) between successive parallel crystalline planes. From these data the estimated average value of lattice parameter (a) of Ag NPs crystal is calculated using the well-known relation:

$$a = d\sqrt{h^2 + k^2 + l^2}, \quad (3)$$

where h, k and *l* are the Millar indices corresponding to the diffraction plane (hk*l*).

From XRD data d is calculated using Bragg's equation:

$$d = \frac{\lambda}{2\sin\theta}, \quad (4)$$

where λ is the wavelength of the X-ray used and θ is Bragg angle corresponding to the diffraction plane.

Following these two equations interplanar distance (d) and lattice constant (a) were calculated and a comparison was made between the standard value [39,40] and the result obtained from SAED and XRD analysis as given in Table 2. Result shows that both 'a' and 'd' obtained from XRD and SEAD measurements follow the standard value, confirming the sample is made of pure Ag. Moreover, the XRD result is closer to the standard value than the SAED result and is consistent with others [40].

2. Morphological and Chemical Composition Analysis

2-1. SEM and EDS Studies

Again, to study the morphological and chemical constituents of the Ag NPs, we have used SEM and EDS. From the SEM image of the sample for concentration of Guava leaf extract of 4 ml [Fig. 6(a)], it is observed that the NPs are spherical with almost uniform size. It is also observed that the Ag NPs are agglomerated. Such agglomeration is due to the drop casting of the particles dispersed in water on the aluminum surface. The EDS spectrum [Fig. 6(b)] shows a strong peak of Ag, which confirms that the synthesized NPs are composed of Ag. The other peaks in the EDS spectrum are due to the Al plate in which the film was prepared to study EDS and also may be because of the residual biomolecules present in the sample. These data are in very good concurrence with the XRD and TEM data.

3. Spectroscopic Analysis

3-1. OA Spectroscopy Studies

During preparation of the samples the color of the aqueous solution of silver nitrate changed gradually from colorless to light yellow and finally blackish brown with increasing concentration of Guava leaf extract. Such changes in color are caused by the formation of Ag NPs with different sizes. Moreover, the faster change in

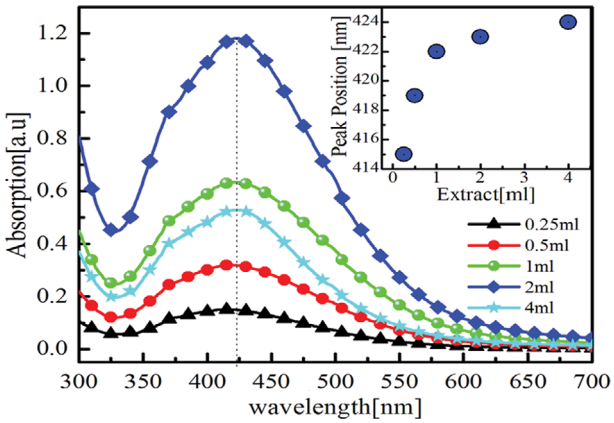

Fig. 7. Optical absorption spectra of Ag NPs for different leaf extract concentrations. Inset shows the shift in peak position of maximum absorption with leaf extract concentration.

color for the samples having higher amount of leaf extract concentration was observed during formation of Ag NP. This is due to the rapid nucleation and faster growth of the particles. The genesis of Ag NPs can be confirmed by measuring the OA spectra of the colored aqueous solution which is the most essential and elementary techniques. In Fig. 7 the OA spectra are plotted for a preparation time of 3 hours after adding 0.25 ml, 0.5 ml, 1 ml, 2 ml, and 4 ml Guava leaf extract in 50 ml of 0.001 M silver nitrate aqueous solution. For the sample with 0.25 ml leaf extract, a peak in the OA spectrum is seen at ~415 nm. This OA peak appears resulting from the absorption due to surface plasmon resonance (SPR) of Ag NPs [41], authenticating the genesis of Ag NPs and are in line with the observed data of XRD and TEM. An increase in OA peak intensity with a corresponding shift towards higher wavelength (redshift) with increase in concentration of leaf extract is observed. The wavelength corresponding to maximum absorption for all the five samples with respect to leaf extract concentration is plotted as an inset in Fig. 7. Here it is clearly observed that initially the absorption maxima redshifted rapidly with the increase in leaf extract and finally attained almost saturation. It is evidently observed that a redshift in wavelength corresponding to maximum absorption from 415 nm to 424 nm has been estimated as the concentration of leaf extract raised from 0.25 ml to 4 ml in 50 ml aqueous silver nitrate solution. It was also found that the FWHM of the absorption spectra gradually decreased with the increase of Guava leaf extract concentration in the precursor solution. This redshift in OA peak with corresponding reduction of FWHM is due to the growth of Ag NPs [42]. Since, redshift corresponds to increase in particle size, the sample having 4 ml leaf extract in 50 ml aqueous silver nitrate solution synthesized largest particle among the rest. This observation is in accordance with the result obtained through TEM and XRD studies. Here, the OA spectra are not normalized and hence the absorbance of 2 ml leaf extract sample is more than 4 ml sample. This explanation is also valid for the sample having 1 ml leaf extract.

The growth of Ag NPs of S5 sample (highest concentration of leaf extract considered here) with different time interval (in the range of 0 min-2,880 min) was studied and plotted in Fig. 8. It is noticed from the figure that as the time increases the peak of the absorption intensity increases, whereas FWHM decreases, which indicates the growth as well as production of Ag NPs. The variation of wavelength corresponding to maximum OA for this sample with natural logarithm of time is shown in the inset of Fig. 8. Here it is also observed that initially a redshift occurs in the absorption maxima and finally it becomes almost a constant in time. This study clearly indicates that initially Ag NPs grow faster and then saturate to a fixed size.

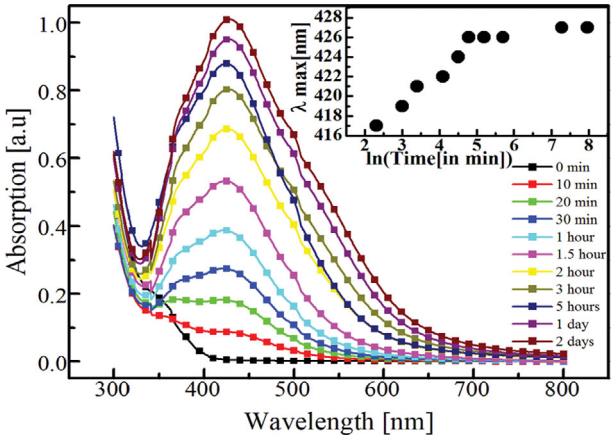

Fig. 8. Optical absorption spectra of Ag NPs for different time interval of S5 sample. Inset shows the shift in peak position of maximum absorption with time.

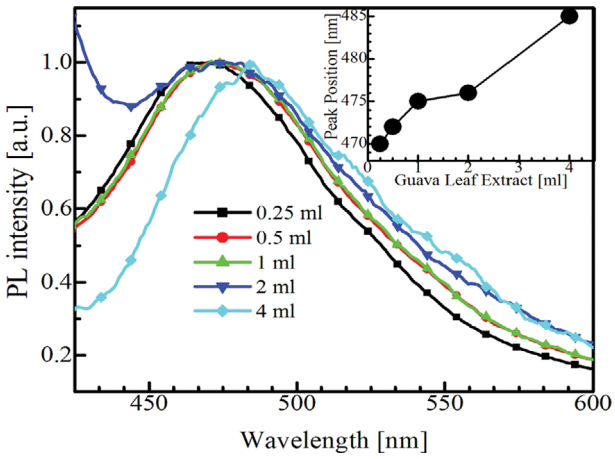

Fig. 9. PL spectra of Ag NPs for different Guava leaf extract concentrations. Inset shows the variation of peak position as a function of leaf extract. Solid line is to guide the eye.

3-2. Photoluminescence (PL) Studies

All the five samples of Ag NPs water suspension were used to carry out photoluminescence studies and the corresponding results in the form of PL spectra are shown in Fig. 9. For all the PL spectra, the intensities had been normalized to unity. For S1 sample a wide PL emission peak appeared at ~470 nm. With the increase of leaf extract concentration a red shift from 470 nm (S1) to 485 nm (S5) was observed as shown in the inset of the same figure. As leaf extract concentration increases, NP sizes also increase, resulting in a systematic redshift in the PL spectra as observed in the UV spectra for the same samples.

The appearance of PL emission peak is well explained by Verma et al. [41]. Such PL spectra appear due to inter-band transition, which is ascribed to recombination of electrons in sp band with the holes in d band. The observation of PL emission of Ag NPs is in coherence with the results of others [34,43]. The observed redshift of the emission peak with increase in NP size is also in line with Parang et al. [43].

3-3. Fourier Transformed Infrared (FTIR) Spectroscopy Studies

The FTIR spectra of all the samples including the leaf extract are shown in Fig. 10. FTIR analysis confirms the presence of the functional groups in the leaf extract responsible for playing role as reducing agent in Ag NP formation. Again, among the different biomolecules present in the leaf extract, flavonoid is the strongest reducing agent which can speed up the reduction of Ag^{+} ions to Ag NPs. The spectrum corresponding to sample S0 shows a broad absorption peak at ~3,450 cm^{-1} corresponding to O-H and vibrational

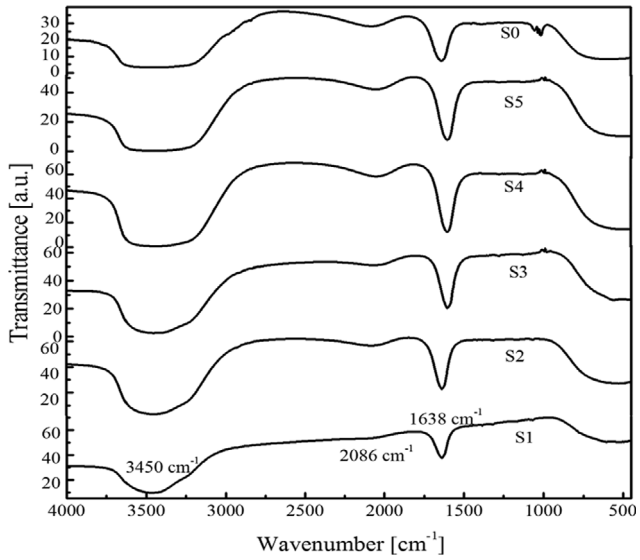

Fig. 10. FTIR spectra of Ag NPs for different Guava leaf extract concentrations.

stretching [44], the absorption dip at 2,086 cm^{-1} and 1,638 cm^{-1} assigned as -C=C- stretching and -C=O stretching, respectively [45]. As shown in the figure, the band centered at 3,450 cm^{-1} has become narrower after the formation of Ag NP. This transformation may be due to the breakage of H-bonds between the hydroxyl groups present in the biomolecules of the leaf extract which get absorbed on the exposed surface of Ag NPs and try to make strong bonds with Ag atoms, leading to stabilizing the NPs [46,47]. Thus, after the formation of Ag NPs the concentration of O-H functional group in the sample reduces and hence a relatively narrow band in the FTIR spectra is observed.

4. Antimicrobial Study

The antibacterial performance of Ag NPs evaluated against *E. coli* is represented in Fig. 11. It has already been reported that Gram negative *E. coli* showed a greater sensitivity by comparison with that of Gram positive *Bacillus subtilis* due to a very thin peptidoglycan layer of Gram negative bacteria from Gram positive one [48]. Thus, our study of antibacterial effect was focused on *E. coli*.

All the Ag NP solutions (S1, S2, S3, S4 and S5) show significant increase in inhibitory effect in terms of increased inhibition zone diameter against tested *E. coli* strain than aqueous $AgNO_3$ solution (sample S0). The diameter of ZOI is gradually increased from S5 to S1, indicating that size of Ag NP matters. Fig. 11(a) shows the relative graph of the size controlled antimicrobial behavior of Ag NPs towards the *E. coli*. Smallest Ag NPs of average size ~13.8 nm show highest inhibition zone as compared to the largest Ag NPs (size ~21 nm), against same concentration of *E. coli*. This result is a complete study for size dependent antimicrobial behavior of Ag NPs, which shows that this activity is extremely reliant on the size of Ag NPs. This may be attributed to the increase in surface-to-volume ratio (STVR) with decrease in NP size. As size decreases, the overall STVR of Ag NPs increases. This means that smaller Ag NPs having larger interactable surface area function as more efficient antibacterial agents than others [48].

Fig. 11(b) shows that the Ag NPs of size ~13.8 nm shows greater antibacterial effect as compared to the chemically synthesized PVP capped Ag NPs. During synthesis, individual NPs interact with one another via physical adhesion and weak forces, resulting in agglomeration. This agglomeration strictly inhibits the overall antibacterial effect [49]. In the process of green NP synthesis, biomolecules not only function as reducing agent but also form a monolayer on the surface of NPs to check the agglomeration. These biological coating agents also act to reduce the toxicity and improve antimicrobial action [50].

From the result showed in Fig. 11(b) it was also depicted that green synthesized Ag NPs show better antibacterial effect than aqueous $AgNO_3$ and Guava extract also. This improved antimicrobial effect of green synthesized Ag NPs is due to the synergistic effect between biomolecules and NPs present in the sample [51].

Only 13.8 nm sized Ag NPs (S1) were considered for MIC evaluation due to their highest efficiency. The lowest strength of Ag NPs where microbial growth absorbance value significantly reduced to zero, was measured as 40 μg/ml. Hence, the MIC of Ag NPs having size 13.8 nm against *E. coli* was determined as 40 μg/ml. From

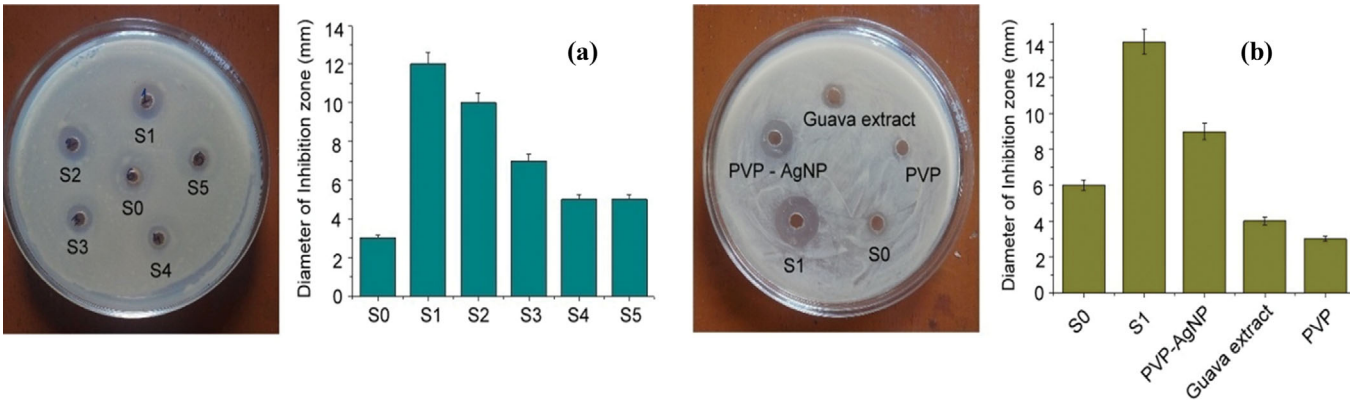

Fig. 11. Antibacterial effects of Ag NPs against *E. coli*; (a) zone of inhibition of samples S1 to S5, showing small sized Ag NP has greater effect than larger one, (b) green synthesized Ag NP (S1) has greater antibacterial effect than aqueous $AgNO_3$ (S0), chemically, i.e., PVP synthesized $AgNO_3$ and guava extract.

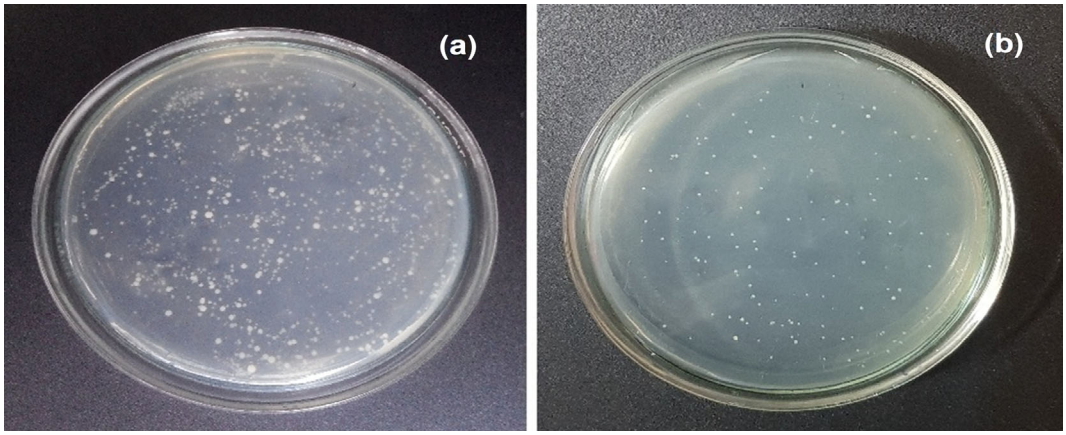

Fig. 12. Viable plate count of *E. coli*; (a) Agar plate showing colony of normal untreated *E. coli*, (b) Agar plate showing colony of Ag NP treated *E. coli* culture.

those tubes viewing no visible growth MLC was determined and it was found as 80 μg/ml.

Viable plate count (Fig. 12) shows significant reduction in colony number for Ag NPs treated *E. coli* culture from that of the normal *E. coli* culture. After 24 hr incubation colony numbers found to be 247 for test 1, i.e., untreated culture and 116 for test 2, i.e., Ag NP treated culture. From that colony number CFU/ml was calculated as 1.24×10^7 and 5.8×10^6 for test 1 and test 2, respectively. The survival percentage was found to be 47%.

5. Probable Mechanism of Synthesis of Ag NPs

The addition of Guava leaf extract in the transparent $AgNO_3$ solution changes its color, confirming the formation of Ag NPs as seen in the top panel of Fig. 13. Here the presence of different bio-molecules in Guava leaf extract acts as a natural reducing and stabilizing agent. The main constituents of the leaf extracts are flavonoids, Eugenol, Tannins, Chlorophyl, cinol, curcumene, terpenoids, menthol, Isopropyl alcohol, β-Caryophyllene, Nerolidol [52]. It has been reported that the presence of flavonoids in the leaf extract reduces Ag^+ ions to Ag and thereby acts as a reducing as well as capping agent in the formation of Ag NPs [53].

The exact mechanism of flavonoid role as a reducing and capping agent in formation of Ag NPs is still to be unveiled. Makarov et al. [54] proposed that the presence of different types of -OH groups in flavonoids plays a significant role to reduce the Ag^+ ion to Ag atom and capping it through chelating by close presence of functional groups, i.e., hydroxyl and carbonyl and also by catechol

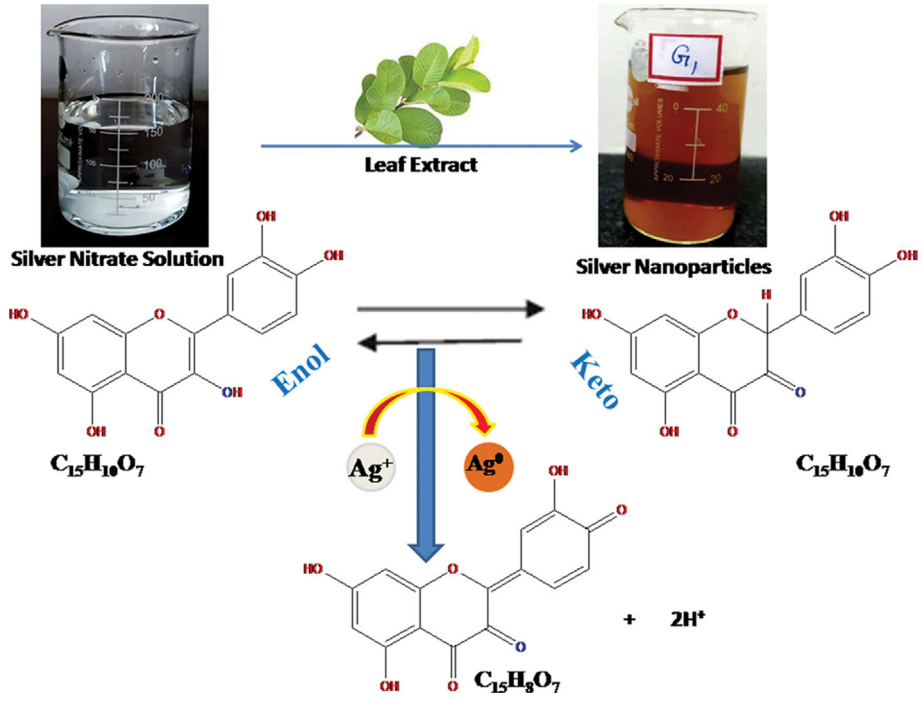

Fig. 13. Probable mechanism of reduction of Ag^+ ions and formation of Ag NPs.

moiety of flavonoids. Ahmad et al. [55] also reported that the tautomeric transformation between keto and enol forms of flavonoids may release a reactive hydrogen atom, resulting in the reduction of metal ions to metal NPs. Again, the density-function theory (DFT) study of Trouillas et al. [56] suggested that the bond-dissociation energies of O-H bond of catechol moiety of flavonoids are less than the other -OH groups present in flavonoids, and hence -OH groups of catechol moiety of flavonoids may take part in metal ion reduction. The above explanation justifies the result obtained in the FTIR spectra. In the FTIR spectra of the leaf extract, a broad peak of -OH appeared due to the abundant presence of the -OH functional group in flavonoids. The peak became narrower after Ag NP formation, which may be attributed to the usage of functional group -OH in the reduction process.

Considering all these possible reductions of Ag^+ ions to Ag^0 and capping them to produce Ag NPs is sketched as in Fig. 13.

CONCLUSION

Ag NPs of average sizes in the range of ~21 nm to ~14 nm were synthesized following green synthesis route using Guava leaf extract of different concentrations. Complementary studies (employing XRD, TEM, SEM, and OA spectroscopy) confirmed that the Ag NPs were fcc in crystal structure and spherical in shape. The average size of the NPs increased with increase in concentration of leaf extract. An extensive study on size dependent antibacterial effects of these NPs was carried out using *E. coli* bacteria. Antibacterial efficiency was found to be greater for smaller NPs compared to larger NPs. This was mainly due to large STVR of small particles. Also, it was confirmed that Ag NPs synthesized following green route was more efficient than the chemically synthesized (PVP capped) Ag NPs. Subsequently, Ag NPs can be successfully used in biomedical applications safely, as these are prepared through green synthesis approach. The probable mechanism of bio-reduction of silver ions and formation of Ag NPs has also been well explained, which justifies the result obtained in the FTIR spectra.

ACKNOWLEDGEMENTS

The authors gratefully acknowledge the University Science Instrumentation Centre of the University of Burdwan for extending the SEM, EDS, and TEM facilities.

CONFLICT OF INTERESTS

The authors have no conflicts of interest to declare that are relevant to the content of this article.

FUNDING

No funds or grants were received for the present study.

DATA AVAILABILITY

The authors declare that all the data supporting the findings of this study are available within the article.

ETHICAL APPROVAL

Authors declare that this manuscript is compliance with scientific ethical standards. There are no other persons who satisfied the criteria for authorship but are not listed. We further confirm that the order of authors listed in the manuscript has been approved by all of us.

REFERENCES

1. S. Prabhu and E. K. Poulose, *Int. Nano Lett.*, **2**, 32 (2012).
2. S. Ghosh, S. Patil, M. Ahire, R. Kitture, S. Kale, K. Pardesi, S. S. Cameotra, J. Bellare, D. D. Dhavale, A. Jabgunde and B. A. Chopade, *Int. J. Nanomedicine*, **7**, 483 (2012).
3. H. H. Lara, E. N. Garza-Trevino, L. Ixtepan-Turrent and D. K. Singh, *J Nanobiotechnology*, **9**, 30 (2011).
4. M. Rai, A. Yadav and A. Gade, *Biotechnol. Adv.*, **27**, 76 (2009).
5. H. J. Klasen, *Burns*, **26**, 17 (2000).
6. I. Sondi and B. Salopek-Sondi, *J. Colloid Interface Sci.*, **275**, 177 (2004).
7. H. H. Lara, N. V. Ayala-Nunez, L. Ixtepan-Turrent and C. Rodriguez-Padilla, *J. Nanobiotechnology*, **8**, 1 (2010).
8. M. C. Daniel and D. Astruc, *Chem. Rev.*, **104**, 293 (2004).
9. S. Lee, E. J. Cha, K. Park, S. Y. Lee, J. K. Hong, I. C. Sun, S. Kim, K. Choi, I. C. Kwon, K. Kim and C. H. Ahn, *Angew. Chem. Int. Ed.*, **47**, 2804 (2008).
10. A. H. A. Kelkawi, A. A. Kajani and A. K. Bordbar, *IET Nanobiotechnol.*, **11**, 370 (2017)
11. Z. Muhammad, A. Raza, S. Ghafoor, A. Naeem, S. S. Naz, S. Riaz, W. Ahmed and N. F. Rana, *Eur. J. Pharm. Sci.*, **91**, 251 (2016).
12. S. Agnihotri, S. Mukherji and S. Mukherji, *RSC Adv.*, **4**, 3974 (2014).
13. R. Dobrucka and J. Długaszewska, *Indian J. Microbiol.*, **55**, 168 (2015).
14. Y. Jeong, D. W. Lim and J. Choi, *Adv. Mater. Sci. Eng.*, **2014**, 763807 (2014).
15. K. Vasilev, *Coatings*, **9**, 654 (2019).
16. M. Casolaro, I. Casolaro, J. Akimoto, M. Ueda, M. Ueki and Y. Ito, *Gels*, **4**, 42 (2018).
17. O. Kvitek, E. Mutylo, B. Vokata, P. Ulbrich, D. Fajstavr, A. Reznickova and V. Svorcik, *Coatings*, **10**, 1046 (2020).
18. L. Petrova, O. Kozlova, E. Vladimirtseva, S. Smirnova, A. Lipina and O. Odintsova, *Coatings*, **11**, 159 (2021).
19. S. Mahmud, M. Z. Sultana, M. N. Pervez, M. A. Habib and H. H. Liu, *Fibers*, **5**, 35 (2017).
20. S. Mukherji, S. Bharti, G. Shukla and S. Mukherji, *Phys. Sci. Rev.*, **4**, 20170082 (2018).
21. A. Shahzad, W. S. Kim and T. Yu, *RSC Adv.*, **5**, 28652 (2015).
22. A. Shahzad, M. Chung, T. Yu and W. S. Kim, *Chem. Asian J.*, **10**, 2512 (2015).
23. H. J. Han, T. Yu, W. S. Kim and S. H. Im, *J. Cryst. Growth*, **469**, 46 (2017).
24. F. Hussain, S. M. Shaban, J. Kim and D. H. Kim, *Korean J. Chem. Eng.*, **36**, 988 (2019).
25. K. Seku, B. R. Gangapuram, B. Pejjai, K. K. Kadimpati and N. Golla, *J. Nanostruct. Chem.*, **8**, 179 (2018).
26. M. R. Khodadadi, M. E. Olya and A. Naeimi, *Korean J. Chem. Eng.*,

33, 2018 (2016).
27. P. K. Kuiri and D. P. Mahapatra, *Adv. Sci. Eng.*, **6**, 290 (2012).
28. P. K. Kuiri, *J. Appl. Phys.*, **108**, 054301 (2010).
29. P. Raveendran, J. Fu and S. L. Wallen, *J. Am. Chem. Soc.*, **125**, 13940 (2003).
30. P. Roy, B. Das, A. Mohanty and S. Mohapatra, *Appl. Nanosci.*, **7**, 843 (2017).
31. J. M. Wiley, L. M. Sherwood and C. J. Woolverton, *Prescott's microbiology*, 9th Ed., McGraw Hill International (2013).
32. T. Ghosh, A. Chottopadhyay, A. C. Mandal, S. Pramanik and P. K. Kuiri, *Chin. J. Phys.*, **68**, 835 (2020).
33. M. Goudarzi, N. Mir, M. Mousavi-Kamazani, S. Bagheri and M. Salavati-Niasari, *Sci. Rep.*, **6**, 32539 (2016).
34. J. Siddhant and M. S. Mehata, *Sci. Rep.*, **7**, 15867 (2017).
35. A. L. Patterson, *Phys. Rev.*, **56**, 978 (1939).
36. S. Pramanik, T. Ghosh, M. Ghosh, S. C. De and P. K. Kuiri, *Adv. Sci. Eng. Med.*, **9**, 414 (2017).
37. S. Mukherjee, S. Pramanik, S. Das, S. Chakraborty, R. Nath and P. K. Kuiri, *J. Alloys Compd.*, **814**, 152015 (2020).
38. H. C. Ong, A. X. E. Zhu and G. T. Du, *Appl. Phys. Lett.*, **80**, 941 (2002).
39. M. C. G. Toro, J. P. Schlegel and C. H. C. Giraldo, *Chemistry Select*, **3**, 8936 (2018).
40. W. I. A. Fattah, A. S. M. Sallam, N. A. Attawa, E. Salama, A. M. Maghraby and G. W. Ali, *Mater. Res. Express.*, **1**, 035024 (2014).
41. A. Verma and M. S. Mehata, *J. Radiat. Res. Appl. Sc.*, **9**, 109 (2016).
42. P. K. Kuiri and S. Pramanik, *J. Appl. Phys.*, **123**, 154302 (2018).
43. Z. Parang, A. Keshavarz, S. Farahi, S. M. Elahi, M. Ghoranneviss and S. Parhoodeh, *Scientia Iranica*, **19**, 843 (2012).
44. S. Pramanik, S. Mondal, A. C. Mandal, S. Mukherjee, S. Das, T. Ghosh, R. Nath, M. Ghosh and P. K. Kuiri, *J. Alloys Compd.*, **849**, 156684 (2020).
45. P. R. Sougandhi, M. Reddeppa, S. S. Harini, T. S. Rani and R. Gangadhara, *J. of Drug Delivery and Therapeutics*, **8**, 301 (2018).
46. S. Hemadi and S. A. Shojaosadati, *Polyhedron*, **171**, 172 (2019).
47. A. Jayakumar and R. K. Vedhaiyan, *Korean J. Chem. Eng.*, **36**, 1869 (2019).
48. Y. Qing, L. Cheng R. Li, G. Liu,Y. Zhang, X. Tang, J. Wang, H. Liu and Y. Qin, *Int. J. Nanomedicine*, **13**, 3311 (2018).
49. J. Virkutyte and R. S. Varma, *Sustainable preparation of metal nanoparticles*, Royal Society of Chemistry, Cambridge (2012).
50. A. Roy, O. Bulut, S. Some, A. K. Mandal and M. D. Yilmaz, *RSC Adv.*, **9**, 2673 (2019).
51. N. Durán, M. Durán, M. B. de Jesus, A. B. Seabra, W. J. Fávaro and G. Nakazato, *Nanomedicine: Nanotechnology, Biology and Medicine*, **12**, 789 (2016).
52. U. K. Parashar, V. Kumar, T. Bera, P. S. Saxena, G. Nath, S. K. Srivastava, R. Giri and A. Srivastava, *Nanotechnology*, **22**, 415104 (2011).
53. D. Bose and S. Chatterjee, *Appl. Nanosci.*, **6**, 895 (2016).
54. V. V. Makarov, A. J. Love, O. V. Sinitsyna, S. S. Makarova, I. V. Yaminsky, M. E. Taliansky and N. O. Kalinina, *Acta Nature*, **6**, 35 (2014).
55. N. Ahmad, S. Sharma, M. K. Alam, V. N. Singh, S. F. Shamsi, B. R. Mehta and A. Fatma, *Colloids Surf. B: Biointerfaces*, **81**, 81 (2010).
56. P. Trouillas, P. Marsal, D. Siri, R. Lazzaroni and J. L. Duroux, *Food Chem.*, **97**, 679 (2006).